Journal of Plankton Research Vol.17 no.6 pp.1245–1271, 1995

An estimate of global primary production in the ocean from satellite radiometer data

Alan Longhurst, Shubha Sathyendranath[1], Trevor Platt and Carla Caverhill
Biological Oceanography Division, Bedford Institute of Oceanography, Dartmouth, Nova Scotia, B2Y 4A2 and [1]Department of Oceanography, Dalhousie University, Halifax, Nova Scotia, B3H 4J1, Canada

Abstract. An estimate of global net primary production in the ocean has been computed from the monthly mean near-surface chlorophyll fields for 1979–1986 obtained by the Nimbus 7 CZCS radiometer. Our model required information about the subsurface distribution of chlorophyll, the parameters of the photosynthesis–light relationship, the sun angle and cloudiness. The computations were partitioned among 57 biogeochemical provinces that were specified from regional oceanography and by examination of the chlorophyll fields. Making different assumptions about the overestimation of chlorophyll by the CZCS in turbid coastal areas, the global net primary production from phytoplankton is given as 45–50 Gt C $year^{-1}$. This may be compared with current published estimates for land plants of 45–68 Gt C $year^{-1}$ and for coastal vegetation of 1.9 Gt C $year^{-1}$.

Introduction

Unless the controls on the growth of marine phytoplankton are understood there can be little progress in the general ecology of the oceans. This perception set the priorities of the biological oceanographers of the late 19th century, so that by about 1935 the basic principles of phytoplankton ecology were already understood (Mills, 1989; deBaar, 1994). However, without two technical revolutions there could be no rational estimate of the growth of phytoplankton over long periods and large regions, although this must be one of the central goals of biological oceanography. The two revolutions were, of course, the use of radioisotope tracers to measure the growth of algal cells in natural seawater samples, and the measurement of the global sea-surface chlorophyll field by radiometers carried on earth-orbiting satellites.

The ^{14}C tracer technique was devised and tested by Steeman Nielsen (1952) in a single year prior to the departure of the round-the-world Galathea expedition. The technique proved so robust at sea that 197 multiple-depth ^{14}C uptake stations were worked in all oceans, yielding results ranging from 0.034 g C m^{-2} day^{-1} in the North Atlantic central gyre to 1.92 g C m^{-2} day^{-1} in the Benguela system upwelling zone (Steeman Nielsen and Jensen, 1957).

The ^{14}C technique was rapidly taken up by other groups (see, for example, the ICES, 1958) and remains the method of choice today, despite a lack of standardization and a cascade of methodological criticism, generally tending to suggest that production rates have been underestimated (see, for example, Chavez and Barber, 1987; Martin *et al.*, 1987; Knauer, 1993), or that the fundamental scale of measurement is inappropriate for extrapolation to the global scale (Platt, 1984). Rarely, in fact, can a technique have been so persistently criticized, but so consistently used.

The Galathea data yielded the first rational estimate of global annual primary production (Steeman Nielsen and Jensen, 1957) of 12–15 Gt C $year^{-1}$, extrapolated from a mean value of 0.15 g C m^{-2} day^{-1} for all stations; the only earlier global estimate of 126 Gt C $year^{-1}$ (Riley, 1939), derived from oxygen incubations, was thus shown to be much too high. Fleming (1957) and Gessner (1957) published versions of the Galathea map integrated with a few other ^{14}C data, Gessner inferring a global total of 20 Gt C $year^{-1}$. By 1965, Koblentz-Mishke was able to publish a map of Pacific Ocean productivity based on 3000 ^{14}C tracer stations, and in 1970 to extend this to the now widely reproduced global map based on 7000 data points (by no means all of which were based on the ^{14}C method), from which she computed a global total primary production of 23 Gt C $year^{-1}$. The compilation by Berger *et al.* (1987) of 8000 data points, mostly obtained post-1970, yielded a global total of 26.9 Gt C $year^{-1}$. In 1975, Platt and Subba Rao tabulated all the then published ^{14}C tracer results for each ocean basin, yielding a global total of 31 Gt C $year^{-1}$, which they compared with other estimates made since the introduction of the ^{14}C tracer method.

All other published estimates based on the ^{14}C method [see the tabulation of Sundquist (1985) for example] are secondary, being derived by the application of a correction factor to previous calculations based on the ^{14}C tracer method. Variability in these estimates (among which it would be difficult to choose objectively) reveals a high level of uncertainty. When mass-balance and indirect methods for computing gross global primary production are included in the comparison, the true level of uncertainty for modern computations is even higher [see, for example, Platt *et al.* (1989) and Knauer (1993)]. Unfortunately, this is often not recognized when formulating biogeochemical models of the carbon cycle: for these, zero error in global primary production (and other equally important fluxes) is usually assumed.

It is paradoxical that our knowledge of the distribution of biota in the ocean did not keep pace with our enhanced ability to measure rate processes. A serious source of uncertainty in the estimates of Koblentz-Mishke and of Berger (and hence also in the subsequent secondary estimates) stemmed principally from their lack of data on the characteristic regional, seasonal distribution of algal biomass in the ocean; these were required to guide the extrapolation from even sparser ^{14}C data.

This paradox could only be resolved by a revolution in biomass measurement which, fortunately for the progress of biological oceanography, is now at hand. The CZCS radiometer carried aboard Nimbus 7 from 1978 to 1986 demonstrated that measurement of near-surface chlorophyll was feasible over brief periods, over very fine grids and yet over very large areas.

The chlorophyll field recovered from CZCS data is the only window open to a synoptic view of the phytoplankton biomass field at the global scale, but it is by no means perfect. The signal is not vertically resolved, but is heavily weighted towards the surface (Gordon and McCluney, 1975; Gordon and Clark, 1980), and areas of persistent cloud cover will introduce bias. About 90% of the satellite signal is atmospheric in origin, so small errors in atmospheric correction can translate into large errors in estimated chlorophyll (Morel, 1980; Gordon, 1993).

The precision of satellite retrieval for this mission was at best 35% (Gordon *et al.*, 1983), the CZCS radiometers being especially unreliable in coastal seas where high loads of dissolved organic matter may be interpreted as chlorophyll by the satellite (Sathyendranath and Morel, 1983). Another potential source of error is the fact that 8 years is a very short period from which to establish a climatology for an oceanographic field as complex and variable as sea-surface chlorophyll. We appreciate, however, that the low precision of satellite measurements is partially offset by the large number of observations; that the time scales associated with ship-based observations cannot match the rates of change (over four orders of magnitude in oceanic waters) of the chlorophyll field, leading to aliasing (Platt and Herman, 1983); and that the remote sensing of phytoplankton has the potential for improvement with the next generation of ocean-colour satellites now being prepared.

Despite its shortcomings, the CZCS sea-surface chlorophyll seasonal climatology (1978–1986) reveals the pattern of biomass distribution at the global scale with a previously unattainable detail (Feldman *et al.*, 1989). The general availability of these images proved to be one of the most potent catalysts of biological oceanography since the beginning of the electronic revolution and it was quickly suggested that the data might be used for computing primary production, initially by applying simple relationships between surface chlorophyll and water-column primary production (Smith, 1981; Platt and Herman, 1983; Eppley *et al.*, 1985).

This suggestion was soon implemented through techniques that explored the possibilities of combining remotely sensed data with first principles of algal physiology. These semi-analytical methods were initially limited to cases of uniform biomass distribution with depth, and to linear relationships between photosynthesis and available light, and ignored spectral effects in light transmission and photosynthesis (Lewis *et al.*, 1986; Platt, 1986; Campbell and O'Reilly, 1988). Since then, these models have advanced to the stage where they can deal with non-uniform biomass distribution, non-linear photosynthetic response, and spectral effects in light transmission and photosynthesis (Platt and Sathyendranath, 1988; Morel and Berthon, 1989). Not all the parameters required for implementing these models on a pixel-by-pixel basis are available by remote sensing, and methods have to be devised for extrapolating local measurements of model parameters to large scales (Platt and Sathyendranath, 1988). The advanced models differ from each other less in the philosophy of the approach than in the practical routes adopted for defining the distribution of parameters in space and time.

In these calculations, we extend the approach of Platt and Sathyendranath (1988), who suggested that estimates of primary production at the global scale should be partitioned among biogeochemical provinces (Longhurst, in preparation) rather than being done within an ecological continuum. Our principal aim is to demonstrate how the concept may be applied to the whole ocean and how seasonal, regional estimates of primary production may be made routinely when satellite sea-surface chlorophyll data become available on a continuing basis. We also hope to constrain the estimates of carbon flux through the marine

phytoplankton more realistically than has hitherto been possible by simple extrapolation from a few thousand ^{14}C or apparent oxygen utilization measurements.

Our computations differ from all previous estimates of global marine primary production in one main respect: they are independent of the historical data base of direct measurement at sea of the rate of primary production. Instead, the sole input from ^{14}C measurements are the biomass-specific parameters that define the photosynthetic response of phytoplankton to available light. The normalization to biomass, and the information contained in the parameters on the light response, make the approach more versatile, in the sense that it can be easily adapted to changes in the initial conditions (initial biomass) and in the forcing field (light). The initial conditions are then provided with hitherto unattainable detail using remote sensing, and the forcing field (light at the sea surface) is prescribed on a pixel-by-pixel basis using information on location and cloud cover. Note that the light field at the surface is also accessible to remote sensing (Bishop and Rossow, 1991).

It must be emphasized that these computations produce only an estimate of total primary production, including photosynthesis based both on the uptake of 'new' nitrate, made available by physical processes, and uptake of reduced nitrogen compounds 'regenerated' within the euphotic zone. Because the calculation of regional and basin-scale new production is of greater interest, suggestions have been made for stepping from total to new production; resort may be had to seasonal changes of the nitrate field, and to characteristic ratios (the *f*-ratio) between the new and total regenerated production. In this way, Sathyendranath *et al.* (1991) partitioned total production on Georges Bank with the use of satellite chlorophyll and nitrate data.

Recently, it has been suggested that a lower limit for new production and the *f*-ratio may be obtained by comparing computations made with actual chlorophyll profiles and computations made with uniform profiles (Platt *et al.*, 1995); this technique isolates production occurring in the deep chlorophyll maximum, generally associated with nitrate uptake. Since such a computation does not account for that component of surface-layer production which is also associated with nitrate uptake, it yields only a lower limit. For the North Atlantic, such a computation suggested an overall *f*-ratio of 0.1, which is a reasonable mean value for the euphotic zone.

Chlorophyll data, the local algorithm and *P–I* parameters

Our computations required (i) an algorithm to compute primary production integrated down the water column, (ii) a comprehensive and seasonal data set representing the global surface chlorophyll field and (iii) characteristic parameter values for the photosynthesis–light (*P–I*) relationship and to describe the form of the chlorophyll profile. These requirements had to be met monthly at a sufficient number of grid points to capture the detail of the seasonal chlorophyll field revealed in the CZCS data sets.

Surface chlorophyll data

Climatologies for the period 1978–1986 from the CZCS ocean colour files are made available by NASA Goddard Space Flight Center on a 1°, monthly grid for the whole ocean. The values at each of the 42 732 grid points representing the oceans are derived from all Level 3 (Feldman *et al.*, 1989) values that occurred within $1/\sqrt{2}°$ of the centre of the bin represented by the grid point during each time period (N.Kuring, personal communication). We used these values to recalculate the 440/550 nm (blue–green) ratio corresponding to the biomass value, which was then combined with characteristic profile parameters (discussed below) to recover the entire pigment profile; this approach was developed by Sathyendranath and Platt (1989) and by Platt *et al.* (1991).

Local algorithm

The computations were made in exactly the same manner as already described for our North Atlantic basin-scale computation of primary production (Sathyendranath *et al.*, 1995); appropriate seasonal mean values for three parameters (z_m, σ and ρ', see below) were used along with the chlorophyll values to obtain a profile for each grid point at each time step by the method of Sathyendranath and Platt (1989). The cloud cover climatology of Hahn *et al.* (1987) was used with the relevant sun angle to compute radiation at the sea surface for the 15th day of each month at each grid point using the method of Platt *et al.* (1991).

Parameters of the chlorophyll profile and the P–I relationship

To obtain characteristic values for the parameters describing chlorophyll profiles, we acquired original data for 26 232 chlorophyll profiles from ~60 different sources; these are now archived in the National Oceanographic Data Center, Washington, and the British Oceanographic Data Centre, Bidston. Individual profiles were fitted to a shifted Gaussian distribution function (Platt *et al.*, 1988) to obtain values for the parameters defining the form of each profile. We specified a minimum of six depths on each profile to meet minimal statistical requirements, and established further criteria (see Sathyendranath *et al.*, 1995) to reject profiles with suspect or insufficient data. These specifications eliminated ~15%, leaving us 21 872 fitted profiles to represent all oceans, all seasons (Figure 1).

From these fits, we obtained the profile parameters required by the local algorithm: the depth of the chlorophyll maximum (z_m), the standard deviation around the peak value (σ) and the ratio (ρ') of chlorophyll peak height at z_m to total peak biomass. How we used these 21 872 parameter sets to represent all regions and seasons is discussed below.

For the required parameters of the *P–I* relationship we had recourse to significantly fewer observations; lack of high-quality observations of this relationship is a serious gap in phytoplankton ecology. The available data comprised multiple-depth *P–I* experiments at 1862 North Atlantic stations carried out with incubators having 30 light intensities extending to 600 W m^{-2}, thus obtaining high-quality *P–I* curves (Platt *et al.*, 1980).

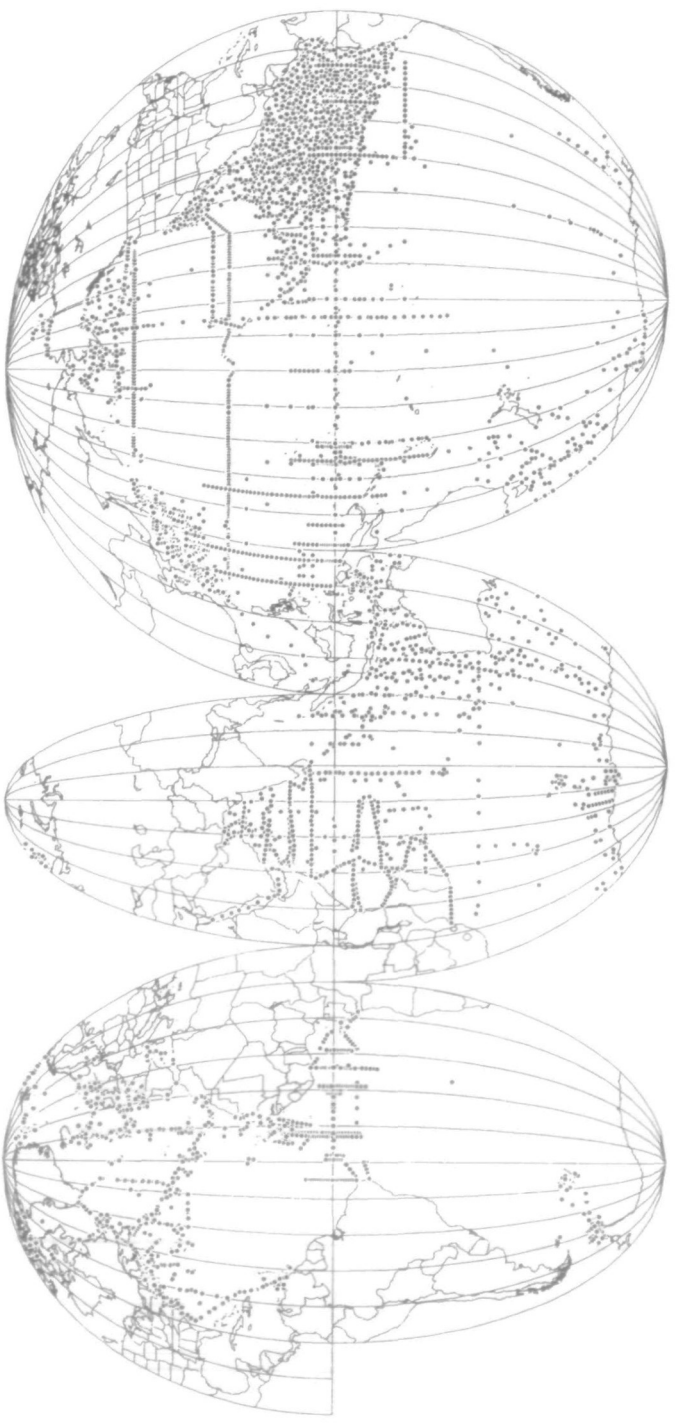

Fig. 1. Distribution of the 21 872 chlorophyll profiles obtained and processed to derive the parameters of the shifted Gaussian model fitted to each profile, required by the local algorithm which was used to compute primary production at each grid point of the chlorophyll field.

From this information we selected characteristic values for the initial slope of the *P–I* curve (α^B) and the assimilation number (P_m^B), both normalized to chlorophyll biomass, to represent polar, westerlies, trade-wind and coastal domains, as described below.

Partitioning the ocean: biogeochemical domains and provinces

The parameter values applied at each grid point are mean values for domains, each supposed to have characteristic seasonal cycles of phytoplankton growth, of the optical field and of the vertical transport of nutrients (Platt and Sathyendranath, 1988; Mueller and Lange, 1989; Platt *et al.*, 1995). Ideally, for use in computation of global production based on routine satellite data, the boundaries between provinces should be variable to accommodate seasonal, annual and decadal-scale changes in the oceanic circulation, and should be bounded by features that can be observed by remote sensing. In this way, their variable location may be monitored along with the sea-surface chlorophyll field. For this demonstration, the province boundaries do not vary seasonally.

A basin-scale test of this concept has already been undertaken for the North Atlantic. To match regional biological oceanography on this scale, it was necessary to recognize a hierarchy of compartments: a small number of primary domains, each partitioned into a larger number of secondary provinces (Sathyendranath *et al.*, 1995). Here, we extend the same logic to the global ocean.

In defining these compartments, we might assume that the primary forcing of algal blooms is associated with mixing rates (and hence nutrient supply), stratification and irradiance at the sea surface; in short, with the terms of the Sverdrup (1953) model, which are indeed necessary conditions for the initiation of a bloom (Platt *et al.*, 1995). However, these are not sufficient conditions to cover all cases: the Sverdrup model was formulated to represent the vernal bloom of the North Atlantic, and assumed forcing of the mixed layer depth only by local wind stress and irradiance at the surface, appropriately enough for the mid-latitudes of the North Atlantic.

Elsewhere in the ocean, the terms of Sverdrup's model insufficiently describe the forcing of algal blooms so, in partitioning the ocean for this demonstration, we have tried to be sensitive not only to the requirements of the Sverdrup model, but also to other factors (discussed below) that determine the seasonality and strength of the algal blooms seen in the CZCS images. This has led us to recognize four primary domains of the global pelagic ecosystem: Polar, Westerlies, Trade Winds and Coastal. These are themselves partitioned into 57 secondary biogeochemical provinces (Figure 2) which we have used as the units of our global computation of primary production. Our arguments for defining these provinces will be fully described elsewhere (Longhurst, in preparation).

Polar domain

The seasonal cycle of sea ice in high latitudes results in a brackish surface layer in

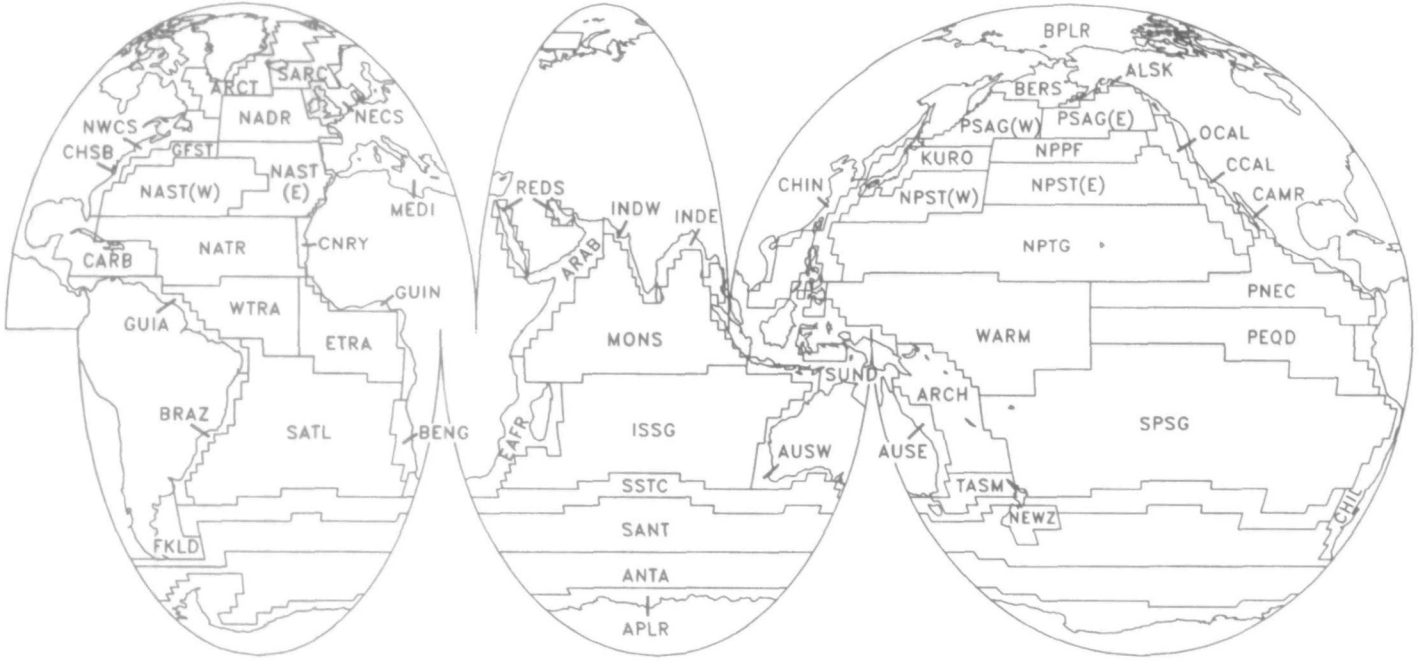

Fig. 2. The 57 biogeochemical provinces used as the compartments for computing seasonal primary production at the global scale; see the text for an explanation of the abbreviations. For the purposes of this computation, boundaries were established on a 2° grid to represent the approximate mean annual shape and location of each province. This approximation suffices for this demonstration, but is a simplification easily improved upon when the method is applied to global sea-surface chlorophyll fields obtained routinely by orbiting radiometers in the future.

spring and summer as freshwater is released from melting winter ice cover; this phenomenon occurs most consistently in the marginal ice zone and leads to an active bloom as soon as ice break-up occurs. However, the phenomenon is also more widespread, as lenses of brackish water are transported throughout the gyral circulation cells that lie north and south of the polar fronts in each hemisphere. The presence, even ephemerally, of a brackish surface layer may induce sufficient stability to initiate an algal bloom as soon as surface irradiance is sufficient. Such blooms occur around Iceland in the same month as the Atlantic vernal bloom at much lower latitudes. This is clearly seen in the analyses of CZCS chlorophyll along 40°W illustrated by Campbell and Aarup (1992).

We are most concerned with this phenomenon in the Southern Ocean and also in the North Atlantic because, for convenience, we regard the Polar or Arctic Ocean as a marginal Atlantic basin. In the North Pacific, it is only in the epicontinental Bering and Okhotsk Seas that the phenomenon is significant. It might be argued that it is illogical to separate the brackish polar surface waters from those of the monsoon regions of the western Pacific; so it would be, but for the fact that the brackish surface layer of the monsoon region is separated by an isothermal 'barrier layer' (Lukas and Lindstrom, 1991) from the deep thermo- and nutriclines. Blooms, therefore, are not normally initiated in relation to the shallow halocline.

Poleward of the polar fronts, we suggest that it is logical to recognize six secondary biogeochemical provinces.

BPLR Boreal Polar. Comprises the Arctic Ocean, Baffin Bay and the Canadian archipelago, and the coastal Greenland and Labrador Currents. It is dominated by permanent ice cover which opens significantly during summer only in some coastal and archipelagic regions.

ARCT Atlantic Artic. This province lies between the Polar Front, lying seawards of the Greenland coastal currents, and the oceanic Polar or Subarctic Front, which often cannot be traced at the sea surface.

SARC Atlantic Subarctic. Comprises the poleward limb of the polar gyre, characterized by warm Atlantic water as it is carried north across the Iceland–Faeroes ridge and thence by the Norwegian Offshore Current into the Barents Sea.

BERS North Pacific Epicontinental Seas. Comprises the Bering Sea and the Sea of Okhotsk, enclosed by the Kuril and Aleutian Islands, respectively, both having extensive areas of continental shelf and a seasonally migrating marginal ice zone.

ANTA Antarctic. Lies between the Polar Frontal Zone and the Antarctic Divergence, having two components: a zone of permanently open water and a zone seasonally carrying pack ice.

APLR Austral Polar. This is a ribbon of westward-moving Antarctic Surface Water, up to 300 km wide, ice covered in winter but with some open water areas in summer, between the Antarctic Divergence and the continent.

Westerlies domain

The defining characteristic of this domain is seasonality in wind stress imposed by the westerlies associated with the Aleutian, Iceland and Antarctic atmospheric low-pressure cells, together with seasonality in the radiation flux at the sea surface. The baroclinicity scale is of order years, rather than weeks, as it is in low latitudes (see discussion of the trade winds domain) and frictional wind stress is translated into eddy motion, rather than momentum. Thus, the defining characteristics of this domain force a deepening of the mixed layer in winter which, in parts of the North Atlantic and elsewhere, may reach to >500 m. In this case, near-surface nitrate levels at the end of winter are in the range 5–10 mmol m^{-3}, setting up the initial conditions for the Sverdrup model of a vernal bloom and its subsequent evolution through summer and autumn conditions.

One of the revelations provided by the first set of global, seasonal CZCS sea-surface chlorophyll fields was that the North Atlantic spring chlorophyll bloom is an exceptional, rather than a typical, process. Spring blooms in other regions can also be detected in the CZCS images, but nowhere does chlorophyll biomass accumulate during spring to the extent familiar in the North Atlantic. Explanations for this discrepancy must be sought in the specific regional oceanographies of each province in this domain: in some cases, as in the northeast Pacific, herbivore control has been inferred (e.g. Parsons and Lalli, 1988); in the Southern Ocean, various controls on the accumulation of algal biomass have been invoked.

Within this domain, we suggest that it is logical to recognize 16 secondary biogeochemical provinces.

NADR North Atlantic Drift. Comprises the North Atlantic Current, lying south of the Oceanic Polar Front and of the Subarctic Front over the Iceland–Faeroe Ridge. To the south, the separation from the northern limb of the subtropical gyre lies at ~40°N.

GFST Gulf Stream. From the Straits of Florida to the Newfoundland Basin. The landward margin is well defined, but the seaward boundary less so. The field of cold core eddies within the warm water of the jet current is included.

NAST North Atlantic Subtropical Gyre (West and East). Comprises the central gyre of the North Atlantic polewards of the subtropical convergence. The mid-Atlantic Ridge constrains the main recirculation gyre within the western basin, and the biological properties of the eastern and western basin are such as to support our subdivision into two provinces.

MEDI Mediterranean, Black Seas. Includes the Mediterranean basin and its marginal seas (Adriatic, Aegean), and also the Black Sea. As for the other

generic mediterranean seas, we do not distinguish between coastal boundaries and oceanic conditions.

PSAG Pacific Subarctic Gyre (West and East). Comprises the Oyashio and Alaska gyres, which can be separated at ~175°E. Useful limits are, to the south, the divergence of surface flow at ~45°N and, to the west, the topography of the Northwest Pacific Rise at 170°E.

KURO Kuroshio Current. Originates in the divergence of the North Equatorial Current east of Luzon, follows the slope of the East China Sea to pass south of Japan. Meanders and flow can then be traced eastwards into the flow of the North Pacific Current; we set the termination at the Northwest Pacific Rise.

NPPF North Pacific Polar Front. A zonal province lying across the North Pacific, north of the Subarctic Boundary of Dodimead *et al.* (1962); it does not include their wider region south of the Alaska gyre.

NPST North Pacific Subtropical Gyre (West and East). Comprises the northern limb of the central gyre originating in the Kuroshio, having somewhat different biological characteristics east and west of 170°E (Venrick, 1979).

OCAL Offshore California Current. From the coastal current westwards to the California Front, or to the canonical boundary of the California Current at 1000 km offshore. The offshore California Current lies progressively closer to the coast towards the south.

TASM Tasman Sea. Between the Subtropical Convergence (from Tasmania around the south of New Zealand) and the edge of the retroflecting East Australian Current eastwards to northern New Zealand.

SPSG South Pacific Subtropical Gyre. Comprises the central and eastern part of the central gyre, bounded to the east by the coastal boundary, and to the north and south by the equatorial divergence and the Subtropical Convergence Zone, respectively. Could undoubtedly be subdivided if more regional oceanography were available.

SSTC South Subtropical Convergence. The most northerly of the annular features of the Southern Ocean. The frontal zone is sufficiently dynamic to have an associated eddy field and includes several surface discontinuity fronts.

SANT Subantarctic. From the Subtropical Convergence south to the Antarctic Polar Front, which is the southern limit of the Polar Frontal zone (previously termed the Antarctic Convergence) and which covers ~4° latitude.

Trade winds domain

The Ekman layer of low latitudes is resistant to wind deepening and the scale of

baroclinicity is weeks, rather than years as in higher latitudes. Characteristically, the shallow tropical pycnocline has very high stability (high values of the Brunt–Väisälä buoyancy frequency, N), associated with a positive heat flux across the sea surface and, in some regions, an excess of precipitation over evaporation. Furthermore, the typical eddy scale is much larger than in higher latitudes so that the value of the Rossby internal radius (R_i) increases equatorwards from 25 km at 50° to 300–400 km at 5° of latitude, as a consequence of the equatorward vanishing of the Coriolis force.

Frictional wind stress in this domain is dominated by the seasonal trade winds, and generates momentum rather than mixing. Western jet currents may spin up (North Brazil Current) or reverse direction (Somali Current) after only a few weeks of modified wind stress, and the depth of the mixed layer is principally determined by seasonal changes in the zonal ridge–trough topography of the pycnocline, reflecting the seasonal shifts in flow of the equatorial current systems.

The extent of the trade wind domain is indicated by zonal discontinuities in the values of N and R_i along the poleward margins of the north and south equatorial currents at ~20–25°N and 15–20°S. Here, N increases rapidly equatorwards from ~6 to ~13 cycles h^{-1}, and R_i from 30–60 to 125–400 km (OceanAtlas software and data; Emery *et al.*, 1984; Houry *et al.*, 1987; and Osborne *et al.*, 1992).

We use such observations to establish the general limits of the trade winds domain along the equatorwards limb of the central gyres of the ocean basins, modified by the specific regional oceanography of each. Within this domain, we expect (i) that mixed-layer algal blooms will not be light limited, (ii) that mixed-layer depth will change seasonally as a geostrophic response to the (often distant) wind field and also to curvature of the wind stress and (iii) that break down of the pycnocline and nutrient renewal in the mixed layer will occur only at strong divergences (as at the equator).

Between the poleward limits of the equatorial currents we recognize 12 secondary biogeochemical provinces that together comprise the trade winds domain.

NATR North Atlantic Tropical Gyre. Comprises the central gyre south of the subtropical convergence zone to the limit of westerly flow along the thermocline ridge at ~10°N marking the northern edge of the North Equatorial Counter-current (NECC).

WTRA Western Tropical Atlantic. The region west of the mid-Atlantic Ridge and between the 10°N thermocline ridge and the subtropical convergence zone.

ETRA Eastern Tropical Atlantic. The Gulf of Guinea (*sensu lato*) eastwards of a meridional boundary at the 20°W hinge-line of the seasonal basin-scale thermocline tilt.

CARB Caribbean. The marginal seas enclosed by the Antillean arc and the Bahamas, extending through the Gulf of Mexico to the Straits of Florida.

SATL South Atlantic Tropical Gyre. Comprises the South Equatorial Current where it forms the equatorward limb of the central gyre.

MONS Indian Ocean Monsoon Gyres. Comprises the gyres (Arabian Sea, Bay of Bengal and south of India) of the transequatorial region of zonal current reversal north of the 10°S thermocline ridge.

ISSG Indian Ocean South Subtropical Gyre. From the south Subtropical Convergence northwards to the hydrochemical front along the 10°S thermocline ridge.

NPTG North Pacific Tropical Gyre. Comprises the southern limb of the central gyre, lying between the Subtropical Convergence and the northern Doldrum front.

PNEC North Pacific Equatorial Countercurrent. Lies along the north slope of the equatorial thermocline ridge, from 80°W westwards across the ocean to ~160°W, where the mixed layer deepens into the western Pacific.

PEQD Pacific Equatorial Divergence. Extends to ~160°W, having minimal meridional extent to the west of 110–120°W. East of these longitudes, asymmetric to the south, extending from ~5°N to ~15°S.

WARM Western Pacific Warm Pool. The low-pressure region of the atmospheric Walker circulation, west of the date line to the Indo-Pacific archipelago, and with a maximum meridional extent (at ~175°E) from 10°N to 20°S.

ARCH Western Pacific Archipelagic Deep Basins. Comprises several minor deep basins mostly within the Sunda shelves: the Andaman, South China, Sulu, Celebes, Molucca, Flores and Banda Seas and, further to the east, the Bismarck, Solomon and Coral Seas.

Coastal domain

We embrace the concept of a coastal boundary domain as defined by Mittelstaedt (1991) for regions where the general oceanic circulation is significantly modified by interaction with coastal topography and with its coastal wind regime. The coastal boundary domain is often bounded by a shelf-break front, and includes coastal upwelling regions and their associated anticyclonic eddy fields. Within the generic mediterranean seas (Caribbean, Red Sea, Bering/ Okhotsk Seas and the deep basins of the archipelagic Indo-Pacific) we cannot, because of the complexity of their regional coastal topography, usefully distinguish a coastal boundary.

It is in the coastal domain that we feel the greatest uncertainty in identifying boundaries between provinces, both because coastal and shelf geography is fractal, so subdivision may be argued at any spatial scale, but also because the

processes that force or constrain algal blooms are more diverse than in the open oceans: river plumes, bathymetric features, bottom roughness, tidal fronts, tidal mixing, local (mountain gap) extreme wind stress, shelf break and coastal upwelling and downwelling. Even this list does not exhaust the possibilities.

With these difficulties in mind, we have restricted the number of provinces in this domain to only 22, although at least twice that number could easily be defined, and perhaps should be. Included in our chlorophyll data is a group of 301 profiles in Chesapeake Bay, in water of ~10 m deep; we exclude these from the coastal boundary domain and reserve them as a model for a global shallow neritic and estuarine zone which we postulate will have to be recognized in an ideal system.

NECS Northeast Atlantic Continental Shelf. From the narrow shelf of western France, north across the British shelf and North Sea, and including also the Baltic Sea where there is seasonal ice cover.

NWCS Northwest Atlantic Continental Shelf. From the anomalously deep shelf of Labrador, the continental shelf shoals progressively southwards and includes two epicontinental seas: the Gulfs of St Lawrence and Maine. Seasonal ice cover occurs in the Labrador Current and the Gulf of St Lawrence.

CNRY Canary Current Coastal. Comprises the seasonally varying regions of coastal upwelling from Cape Finisterre (43°N) to Cap Vert at 15°N, and extending seasonally to the Bissagos Islands at 11°N.

GUIN Guinea Current Coastal. From Guinea-Bissao to Angola at 15°S within the flow of the Guinea Current. Seasonal upwelling occurs off Ghana and the Ivory Coast.

GUIA Guiana Current Coastal. From Cabo de Sao Roque (10°S) in Brazil to Trinidad (10°N) within the offshore limits of the North Brazil (or Guiana) Current along the northern coast of Brazil. Retroflection instability eddies are shed north of the Amazon mouth.

BRAZ Brazil Current Coastal. From the bifurcation of the South Equatorial Current at 10°S, along the South American coast to ~40–42°S where the northward flow of the Falkland Current is encountered. The outer boundary of this rather narrow province seldom occurs beyond the 2000 m contour.

FKLD Southwest Atlantic Continental Shelf. Argentine shelf and Falklands Plateau from Mar del Plata (38°S) to Tierra del Fuego (55°S).

BENG Benguela Current Coastal. From the coastline of Africa out to and including the eddy field offshore from the Benguela Current, and from the Cape peninsula north to Cabo Fria (18°S).

REDS Red Sea and Persian Gulf. Comprises the two semi-enclosed basins of these epicontinental seas, the limits being set at the Bab el Mandeb and the Straits of Hormuz, respectively.

ARAB Northwest Arabian Upwelling. The coastal areas of the northwest Arabian Sea from Somalia to Pakistan. The upwelling region extends from the coastline to an offshore convergence zone.

EAFR East Africa Coastal. From northern Kenya to the Cape of Good Hope, including the Mozambique Channel and east Madagascar. For convenience, we include the Agulhas Retroflection, south of Africa, in this province.

INDE Eastern India Continental Shelf. Comprises the coastal regions over and adjacent to the continental shelf of the Bay of Bengal from Sri Lanka in the west to the Irrawaddy delta.

INDW Western India Continental Shelf. From the mouth of the Indus at 25°N to the Gulf of Mannar at ~7°N, comprising the continental shelf of western India; seasonal upwelling occurs during boreal summer.

AUSW Australia–Indonesia Coastal. The coastal boundary from northern Sumatra to southern Australia including the anomalous southerly flow of the Leeuwin Current; includes the offshore eddy field off Western Australia.

ALSK Alaska Downwelling Coastal. Extends from 53°N (Queen Charlotte Sound) to the end of the Aleutian islands at ~170°W, and from the velocity maximum of the rim current to the coastline.

CCAL California Upwelling Coastal. Inshore of the velocity maximum of the equatorward flow of the California Current from Vancouver Island to Baja California. To the south, bounded by the convergent front southwest of Baja California, and to the north by the divergence of the North Pacific Current south of Vancouver Island.

CAMR Central American Coastal. From the tip of Baja California (Cape San Lucas) to the Gulf of Guayaquil in Ecuador. For convenience, we include the narrow epicontinental sea of the Gulf of California.

CHIL Chile–Peru Current Coastal. Defined, like its Benguela homologue, as extending from the coastline to (and including) the offshore anticyclonic eddy field. To the south, it is defined by the divergence zone at ~45°S and to the north at its separation from the coast near the equator.

CHIN China Seas Coastal. The Yellow and East China Seas from the Korea Straits to ~18°N, near Hainan. The offshore limit is the landward eddy field of the Kuroshio Current.

SUND Sunda–Arafura Seas Coastal. Comprises the extensive continental shelves

between Burma, South China and Australia, including the Gulfs of Tonkin and Thailand and also the smaller shelf areas throughout archipelagic Malaysia, Indonesia and the Philippines.

AUSE Eastern Australia Coastal. Coral Sea coasts of Australia (south to Cape Howe at ~38°S) and New Caledonia. Includes the Great Barrier Reef and other coral formations.

NEWZ New Zealand Coastal. The continental shelf around New Zealand, together with the area within the 1000 m isobath on the New Zealand Plateau and the Chatham Rise.

An estimate of global primary production

To compute global primary production by the application of the local algorithm we require, at each grid point and time step, three parameters for the chlorophyll profile, two for the *P–I* relationship, and a measure of incident radiation.

Using boundaries established on a 1° grid as shown in Figure 2, our 21 872 sets of chlorophyll profile parameters were partitioned among the 57 biogeochemical provinces. We found that the number of data points was insufficient to represent monthly time steps, so we used quarterly intervals centred on the 15th days of January, April, July and October. For the 228 possible cases (57 provinces, four seasons) there are >25 profiles (and therefore parameter sets) for 163 cases; of the remaining 65, there were 22 for which we had no profiles. We examined the variance of the parameter values in the remaining 43 cases and where this took a low value, and appeared reasonable by comparison with neighbouring cases, it was accepted. For the 22 missing values, and for those other cases whose variance was high, we interpolated a value from other regions or seasons as suggested by a consideration of regional oceanography.

For example, we had only 13 profiles for the North Pacific Subtropical Gyre (East), so we interpolated values for the adjacent Offshore California Current province for which we had adequate seasonal coverage. This is not an ideal procedure, but we justify it by the circumstances of this demonstration, and because the potential effects on the final computation are probably small compared with the effect of exchanging the chlorophyll field between adjacent provinces. In this way, we obtained four seasonal values for the profile parameters that, we believe, describe the seasonal chlorophyll profile in each of our 57 provinces sufficiently well for the present purposes.

The same procedure was used for the *P–I* parameters, but at the level of domains, not provinces, although even at this level the available high-quality data were less than ideally distributed, and we have to extrapolate from data obtained in the North Atlantic. The selection of characteristic seasonal values for each domain is discussed by Sathyendranath *et al.* (1995): the same range of values and the same logic for selecting values characteristic of each domain were used for this global calculation. Again, we justify this less than ideal situation by the relatively low variance of the *P–I* parameters (maximum/minimum for α^B is

4.3 and for P_m^B only 3.2 for all cases, e.g. domains, seasons) compared with variance in the chlorophyll biomass field.

Using the Hahn cloud cover climatology (see above) and sun angle, we computed mean monthly production (as mg C m^{-2} day^{-1}) at each grid point for all oceans, the final result being expressed as a weighted mean (based on the area represented by each grid point) for each biogeochemical province. The production values were then integrated over the year for the whole ocean to obtain global water column primary production (as Gt C $year^{-1}$). For those few grid points where CZCS chlorophyll estimates were unavailable (cloud cover, radiometer inactive), the weighted mean of the province representing that month was used in the global integration as the production value at that grid point.

To accommodate seasonal darkness and ice cover in polar latitudes, we assumed nil production for each grid point on days when the sun did not rise. We compared the regions where CZCS pixels showed a data value with the polar ice cover climatology for 1978–1987 (almost the CZCS years) of Gloersen *et al.* (1992), and concluded that in the CZCS climatology only small polar areas were void of data or cloud covered. We could therefore assume that the CZCS polar chlorophyll field approximately indicated the area of open water each month. For the ice-covered regions during the sunlit season, we assumed that no production occurred; the real value is low.

The results of these computations are shown in Table I and Figure 3. We have corrected neither for phaeopigments, theoretically integrated with chlorophyll by the radiometer, nor for suspended sediments and dissolved organic matter in coastal water.

Phaeopigments are now known to be present only at much lower concentrations than indicated by Turner™ fluorometry, the measure of choice for most observers in the past. Morel and Berthon (1989) surveyed many mostly pre-HPLC profiles and were led to suggest that phaeopigments comprised 20–35% of the total pigment signal in all ocean areas. Much of the Turner™ 'phaeopigment' signal is now known to comprise acid-enhanced fluorescence of eukaryotic chlorophyll *b* and prokaryotic divinyl chlorophyll *b* (E.J.H.Head, Bedford Institute, personal communication), thus accounting for the deep 'phaeopigment' maxima observed slightly deeper than the 'chlorophyll' maximum in, for example, the eastern Pacific (Love, 1971).

Modern HPLC pigment data frequently indicate very low, or undetectable, phaeopigments in the open ocean, except during bloom situations or in association with a subsurface pigment peak invisible to the CZCS radiometer. Even when phaeopigments are detectable by HPLC in the open ocean, they usually comprise only 1–5% of total plant pigments, rarely reaching 10% (Gieskes *et al.*, 1988; Strom and Welschmeyer, 1991; Barlow *et al.*, 1993; Head and Horne, 1993; Letelier *et al.*, 1993).

However, in coastal areas, HPLC-determined phaeopigment may be a significant fraction (usually 5–25%) of total plant pigments (e.g. Gieskes and Kraay, 1986; Gieskes *et al.*, 1988), even higher fractions than this (around 50%) being reported at the Antarctic coast (Bidigare *et al.*, 1986), in or below the subsurface chlorophyll maximum. We infer from these results that we may

Table I. Areas of biogeochemical provinces, and some larger areas, with their mean daily and annual rates of net primary production based on the CZCS 1978–1986 climatological data. The last two columns show the effect of assuming that only 50 and 25% of the water-leaving radiation represents chlorophyll in coastal provinces where surface water is likely to be turbid because of the presence of particles other than algal cells. The subset 'upwelling' comprises the four eastern boundary current provinces and ARAB, the coastal province of the northwest Arabian Sea

Domain	Ocean	Province	Area (10^6 km^2)	Primary production rate			Case 2 *0.5	Case 2 *0.25
				g C m^{-2} day^{-1}	g C m^{-2} year^{-1}	Gt C year^{-1}		
Coastal	Atlantic	NECS	1.36	2.00	730	1.00	0.50	0.25
Coastal	Atlantic	NWCS	2.00	1.48	540	1.08	0.54	0.27
Coastal	Atlantic	CNRY	0.81	2.01	732	0.60	0.60	0.60
Coastal	Atlantic	GUIN	1.42	1.36	495	0.70	0.35	0.18
Coastal	Atlantic	GUIA	1.23	1.92	699	0.86	0.43	0.22
Coastal	Atlantic	BRAZ	1.20	0.83	302	0.36	0.18	0.09
Coastal	Atlantic	FKLD	1.42	1.30	474	0.67	0.67	0.67
Coastal	Atlantic	BENG	1.13	0.88	323	0.37	0.37	0.37
Coastal	Indian	REDS	0.56	1.69	617	0.34	0.34	0.34
Coastal	Indian	ARAB	2.93	1.24	454	1.33	1.33	1.33
Coastal	Indian	EAFR	3.72	0.52	190	0.71	0.71	0.71
Coastal	Indian	INDE	0.97	0.97	354	0.34	0.17	0.09
Coastal	Indian	INDW	0.80	1.01	369	0.29	0.15	0.07
Coastal	Indian	AUSW	2.94	0.55	199	0.59	0.59	0.59
Coastal	Pacific	ALSK	0.59	1.81	661	0.39	0.39	0.39
Coastal	Pacific	CCAL	0.96	1.06	388	0.37	0.37	0.37
Coastal	Pacific	CAMR	1.26	0.92	334	0.42	0.42	0.42
Coastal	Pacific	CHIL	2.61	0.74	269	0.70	0.70	0.70
Coastal	Pacific	CHIN	0.97	1.70	619	0.60	0.30	0.15
Coastal	Pacific	SUND	6.33	0.90	328	2.08	1.04	0.52
Coastal	Pacific	AUSE	1.14	0.64	232	0.27	0.27	0.27
Coastal	Pacific	NEWZ	1.04	0.85	312	0.32	0.32	0.32
Polar	Arctic	BPLR	1.66	1.77	645	1.07	1.07	1.07
Polar	Atlantic	ARCT	2.10	1.33	484	1.02	1.02	1.02
Polar	Atlantic	SARC	2.33	0.83	302	0.70	0.70	0.70
Polar	Pacific	BERS	3.89	0.99	363	1.41	1.41	1.41
Polar	Southern	ANTA	8.87	0.45	165	1.47	1.47	1.47
Polar	Southern	APLR	1.93	1.09	398	0.77	0.77	0.77

Westerlies	Atlantic	NADR	3.50	0.66	240	0.84	0.84	0.84
Westerlies	Atlantic	GFST	1.10	0.49	178	0.20	0.20	0.20
Westerlies	Atlantic	NASW	5.80	0.26	95	0.55	0.55	0.55
Westerlies	Atlantic	MEDI	3.08	0.59	216	0.67	0.67	0.67
Westerlies	Atlantic	NASE	4.45	0.33	122	0.54	0.54	0.54
Westerlies	Pacific	PSAE	3.20	0.55	199	0.64	0.64	0.64
Westerlies	Pacific	PSAW	2.90	0.72	264	0.77	0.77	0.77
Westerlies	Pacific	KURO	3.70	0.53	193	0.72	0.72	0.72
Westerlies	Pacific	NPPF	3.02	0.47	172	0.52	0.52	0.52
Westerlies	Pacific	NPSE	6.83	0.30	111	0.76	0.76	0.76
Westerlies	Pacific	NPSW	3.93	0.30	109	0.43	0.43	0.43
Westerlies	Pacific	OCAL	2.39	0.32	117	0.28	0.28	0.28
Westerlies	Pacific	TASM	1.65	0.45	163	0.27	0.27	0.27
Westerlies	Pacific	SPSG	37.29	0.24	87	3.23	3.23	3.23
Westerlies	Southern	SSTC	16.84	0.37	136	2.29	2.29	2.29
Westerlies	Southern	SANT	30.25	0.33	120	3.63	3.63	3.63
Trades	Atlantic	NATR	8.27	0.29	106	0.88	0.88	0.88
Trades	Atlantic	WTRA	5.36	0.36	130	0.70	0.70	0.70
Trades	Atlantic	ETRA	5.34	0.43	157	0.84	0.84	0.84
Trades	Atlantic	SATL	17.77	0.21	75	1.33	1.33	1.33
Trades	Atlantic	CARB	4.48	0.52	190	0.85	0.85	0.85
Trades	Indian	MONS	14.21	0.29	105	1.49	1.49	1.49
Trades	Indian	ISSG	19.25	0.19	71	1.37	1.37	1.37
Trades	Pacific	NPTG	21.09	0.16	59	1.24	1.24	1.24
Trades	Pacific	PNEC	8.17	0.29	107	0.87	0.87	0.87
Trades	Pacific	PEQD	10.34	0.31	113	1.17	1.17	1.17
Trades	Pacific	WARM	16.78	0.22	82	1.38	1.38	1.38
Trades	Pacific	ARCH	8.84	0.27	100	0.88	0.88	0.88
Total			328.0	0.77	282	50.17	46.52	44.70

continued overleaf

Table I. Continued

Geographical subsets	Area (10^6 km^2)	Primary production rate			Case 2 *0.5	Case 2 *0.25
		g C m^{-2} day^{-1}	g C m^{-2} year^{-1}	Gt C year^{-1}		
Coastal domain	37.4	1.1	385	14.4	10.7	8.9
Polar domain	20.8	0.8	310	6.4	6.4	6.4
Westerlies domain	129.9	0.3	126	16.3	16.3	16.3
Trades domain	139.9	0.3	93	13.0	13.0	13.0
Arctic Ocean	1.7	1.8	645	1.1	1.1	1.1
Atlantic Ocean	74.0	0.5	199	14.8	12.8	11.8
Pacific Ocean	148.9	0.4	132	19.7	18.4	17.7
Indian Ocean	45.4	0.4	143	6.5	6.2	6.0
Southern Ocean	57.9	0.4	141	8.2	8.2	8.2
Upwelling provinces	8.4	1.1	398	3.4	3.4	3.4
Atlantic westerlies	17.9	0.4	156	2.8	2.8	2.8
Pacific westerlies	64.9	0.3	117	7.6	7.6	7.6
Atlantic trades	41.2	0.3	112	4.6	4.6	4.6
Pacific trades	65.2	0.2	85	5.5	5.5	5.5
Indian trades	33.5	0.2	86	2.9	2.9	2.9

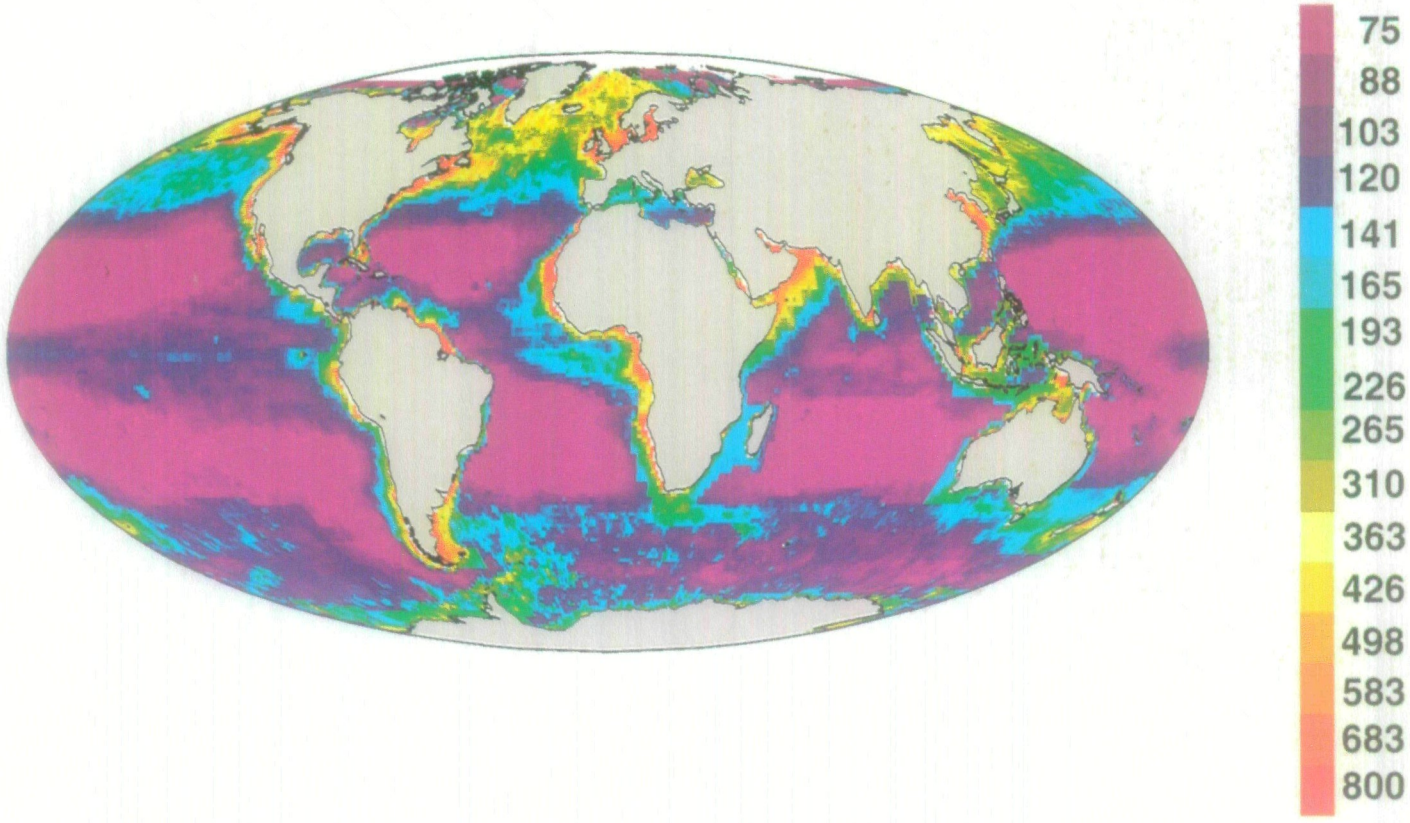

Fig. 3. The annual mean field of total primary production of phytoplankton in the euphotic zone of the oceans (g C m^{-2} y^{-1}) obtained by computation at each grid point of the chorophyll field after assigning characteristic values for each province to all parameters required by the local algorithm.

reasonably ignore the phaeopigment component of the CZCS data in the open ocean, and in coastal waters treat it as part of the general problem of interpreting CZCS data there.

The problem associated with CZCS data in coastal waters admits of no general solution (Sathyendranath and Morel, 1983; Simpson, 1993); we choose to deal with it indirectly by using regional oceanography to separate those coastal provinces having shallow shelf areas, and significant river effluents leading to Case 2 waters in the sense of Morel and Prieur (1977), from those provinces where it is probably trivial. For the purpose of this demonstration, we examine the sensitivity of the global computation to this problem by testing a range of factors to correct for the total radiation signal to one representing only chlorophyll. The direct resolution of this problem must await the availability of data from planned narrow-band-width, multiple-channel radiometers.

Conclusions and comparisons with other estimates

The measure obtained by our calculations is total primary production and is not, of course, the only measure required in quantifying carbon flux; we shall also require to partition this flux into new and regenerated production, and to assess the vertical flux by sinking and entrainment to the interior of the ocean. The value for total primary production in all oceans obtained from our computations (44.7–50.2 Gt C $year^{-1}$) is on the high side of previous estimates, but apparently matches the recent estimate (51 Gt C $year^{-1}$) obtained by extrapolation from a few modern ^{14}C incubations in the eastern Pacific made under ultraclean conditions (Martin *et al.*, 1987; Knauer, 1993).

It has often been the case that convergence between estimates has been understood to indicate mutual support, but a more critical examination of the two estimates in this case suggests that convergence is coincidental. It might be thought that the technical advances associated with the ^{14}C technique used by Martin *et al.* had caused these two modern and quite independent estimates to converge. However, we note that their extrapolation of estimates from three stations to three global 'ocean provinces' was guided by the assumptions of Ryther (1969) concerning the relative areas of open ocean, coastal and upwelling areas. Consequently, the 'upwelling province', over which the productivity rate obtained by Martin *et al.* in the California upwelling was extrapolated, was assumed to have the area (0.36×10^6 km^2 globally) which had been calculated much earlier. Ryther had done this on the basis of an unsupported assumption that the upwelling area off Peru (which was thought to be known from survey data) represented 'no more than one tenth' of the global upwelling area.

There are, of course, many ways of defining upwelling areas: our estimate of the effective upwelling area comprising the five upwelling provinces (ARAB, CCAL, CNRY, CHIL and BENG) totals 8.44×10^6 km^2, which is greater than Ryther's area by a factor of 23. For the same five upwelling areas, Cushing (1969) assumed a total of 4.5×10^6 km^2 and, for all areas where significant upwelling could be detected, a total of 14.9×10^6 km^2, which is 43 times larger than Ryther's upwelling area. Had Martin *et al.* and Knauer extrapolated their

ultraclean data over a more realistic area, their estimate of global primary production would have been much higher than 51 Gt C year^{-1}. Obviously, convergence between global estimates may be more apparent than real, and may have little to do with the methods used to make the original production estimates.

Such a conclusion alone is sufficient justification for the extra labour involved in partitioning our computation of global production. Only by spatial discrimination of this kind will it be realistic to compare computations based on different methods of measuring production, as we shall have to in order to achieve consensus.

Comparing the relative productivity of coastal and oceanic provinces, we calculate that the total production from the oceans is 2.5–4.0 times that of the coastal provinces, depending on the corrections we make for interference with the chlorophyll signal in some coastal zones. The global computation of Berger *et al.* (1987) suggests that the open-ocean production is 1.7 times that in their coastal zone of arbitrary width, while Platt and Subba Rao (1975) calculated that offshore areas had a production almost six times that of their coastal areas, which were defined differently from those of Berger *et al.* It is unprofitable to carry such comparisons too far, or to put too much weight on convergence (or lack thereof) between estimates, because different assumptions concerning the areas over which any experimental result or characteristic value should be extrapolated are surely at least as important to the final result as are methodological differences in the calculations themselves.

However, one difference between our results and those of Berger *et al.* is noteworthy: their computation showed an Atlantic total (5.1 Gt C year^{-1}) less than half that of the Pacific (11.1 Gt C year^{-1}), and about equivalent to the Indian Ocean (4.7 Gt C year^{-1}). Our calculations suggest that production in the Pacific is greater than that in the Atlantic by a factor of only ~1.4, while Platt and Subba Rao estimated a factor of only 1.2. These differences seem to be based on differences both in defining the ocean basins and on different assumptions for regional rates of primary production.

Other regional comparisons are possible, to examine the extent to which estimates are converging as work progresses. Several independent calculations have been made in recent years of production in high latitudes, based on compilations of ^{14}C productivity data. Legendre *et al.* (1992) estimated Arctic production polewards of 65°N as 0.205 Gt C year^{-1}, whereas Platt and Subba Rao (1975) obtained almost the same total for the (largely ice-covered) Arctic Ocean alone. Our estimate, which was corrected for ice cover, for the Boreal Polar, Arctic and Subarctic provinces, a rather larger area, is 2.8 Gt C year^{-1}. For the Antarctic, polewards of 60°S, Legendre *et al.* calculated 2.94 Gt C year^{-1}, including the contribution of growth below the ice. Our estimate for the Antarctic and Antarctic Polar provinces together is 2.24 Gt C year^{-1}, which is fairly close. Perhaps the discrepancy between our estimate and that of Legendre *et al.* for the Arctic region is due to differences in areal extrapolation.

Direct sea-truthing of production estimates made from CZCS data is not possible because the values so obtained are monthly climatologies, while ^{14}C

measurements are date-specific values dependent on the cloudiness and sea state on the actual day of measurement. However, it may be instructive to make the comparison at a higher level of abstraction. Our annual means for the daily primary production rate are 0.3–1.1 g C m^{-2} day^{-1} for the coastal domain, 1.08 for the polar, 0.43 for the westerlies and 0.30 for the trades domain. For the five main upwelling coastal provinces, we obtained annual means of 1.1 g C m^{-2} day^{-1}. Knauer (1993) suggested values of 0.35 g C m^{-2} day^{-1} for the open ocean, 0.68 for the coastal zone and 1.15 for the upwelling regions. Our estimates clearly converge with those of Knauer, but only further comparisons between modern ^{14}C incubations done at sea and new satellite-based computations will prove if this convergence is real, or coincidental.

To put our new estimate of primary production by marine phytoplankton into perspective, we note that ecosystems other than the pelagial contribute only a small fraction of the total global primary production from salt water ecosystems: recent estimates for coral reefs (0.7 Gt C $year^{-1}$; Crossland *et al.*, 1991), coastal macrophytic algae (0.01 Gt C $year^{-1}$; de Vooys, 1979) and salt marshes and estuaries (0.5 and 0.7 Gt C $year^{-1}$, respectively; Woodwell *et al.*, 1973) together add ~4% to our total for the pelagial; the error term for these estimates is probably as large as that for the open oceans. Finally, we note that our estimate of global marine productivity (45–50 Gt C $year^{-1}$) is close to those current for total primary production on land. A recent formal comparison of the output from 17 independent models of net terrestrial primary production (mostly differentiated between 20–30 terrestrial vegetation types somewhat analogous to our biogeochemical provinces) showed that they differed by a factor of ~1.5, ranging from 45 to 68 Gt C $year^{-1}$, or 56 Gt C $year^{-1}$ as a central estimate (Lurin *et al.*, 1994). Too few independent models of marine primary productivity are available for such a formal comparison, but it is not unreasonable to suggest that we can now have some confidence that total global photosynthetic carbon fixation on land and in the ocean is within a factor of 1.5 of 105 Gt C $year^{-1}$.

Acknowledgements

This study could not have been completed without the generous and friendly cooperation of all those who sent us data for chlorophyll profiles; you are too numerous to mention individually, you know who you are, and we thank you. Your data have been archived collectively for access by others unless you requested us not to do this. Karl Banse and Wolfgang Berger offered very helpful suggestions, and we are grateful to them for their assistance. We also thank those who laboured to harmonize and fit the nearly 30 000 chlorophyll profiles we acquired, and who assisted with image analysis: George White, Cathy Porter, Alastair Macdonald. This work is a contribution to the International Space Year Project 'Productivity of Global Oceans' and was supported by the European Space Agency (reference PO 125490); it was also supported by the US Office of Naval Research and the US National Aeronautics and Space Administration. It forms part of the Canadian Department of Fisheries and Oceans contribution to the international Joint Global Ocean Flux Study, and was performed at the Bedford Institute of Oceanography.

References

Barlow,R.G., Mantoura,R.F.C., Gough,M.A. and Fileman,T.W. (1993) Phaeopigment distribution during the 1990 spring bloom in the northeastern Atlantic. *Deep-Sea Res.*, **40**, 2229–2242.

Berger,W.H., Fischer,K., Lai,C. and Wu,G. (1987) Oceanic primary productivity and organic carbon flux. Part 1, Overview and maps of primary production and export. *Scripps Inst. Oceanogr.*, **87–30**, 1–67.

Bidigare,R.R., Frank,T.J., Zastrow,C. and Brooks,J.M. (1986) The distribution of algal chlorophylls and their degradation products in the Southern Ocean. *Deep-Sea Res.*, **33**, 923–938.

Bishop,J.K.B. and Rossow,W.B. (1991) Spatial and temporal variability of global surface solar irradiance. *J. Geophys. Res.*, **96**, 16839–16858.

Campbell,J.W. and Aarup,T. (1992) New production in the North Atlantic derived from seasonal patterns of surface chlorophyll. *Deep-Sea Res.*, **39**, 1669–1694.

Campbell,J.W. and O'Reilly,J.E. (1988) Role of satellites in estimating primary productivity on the Northwest Atlantic Continental Shelf. *Cont. Shelf Res.*, **8**, 179–204.

Chavez,F.P. and Barber,R.T. (1987) An estimate of new production in the equatorial Pacific. *Deep-Sea Res.*, **34**, 1229–1243.

Crossland,C.J., Hatcher,B.G. and Smith,S.V. (1991) Role of reefs in global ocean production. *Coral Reefs*, **10**, 55–64.

Cushing,D.H. (1969) Upwelling and fish production. *U.N. Food Agric. Org. Fish Tech. Paper*, **84**, 1–40.

deBaar,H.J.W. (1994) von Liebigs Law of the Minimum and plankton ecology. *Prog. Oceanogr.*, **33**, 347–386.

de Vooys,C.G.N. (1979) Primary production in aquatic environments. In Bolin,B., Degens,E.T., Kempe,S. and Ketner,P. (eds), *The Global Carbon Cycle*. John Wiley, Chichester, pp. 259–291.

Dodimead,A.J., Favorite,F. and Hirano,T. (1962) Review of the North Pacific Ocean, Part II. *Int. N. Pac. Fish. Comm. Bull.*, **13**, 1–195.

Emery,W.J., Lee,W.G. and Magaard,L. (1984) Geographic and seasonal distributions of Brunt–Väisälä frequency and Rossby radii in the North Pacific and North Atlantic. *J. Phys Oceanogr.*, **14**, 294–317.

Eppley,R.W., Stewart,E., Abbott,M.R. and Heyman,U. (1985) Estimating ocean primary production from satellite chlorophyll. Introduction to regional differences and statistics for the Southern California Bight. *J. Plankton Res.*, **7**, 57–70.

Feldman,G., Kuring,N., Ng,C., Esaias,W., McClain,C.R., Elrod,J., Maynard,N., Endres,D., Evans,R., Brown,J., Walsh,S., Carle,M. and Podesta,G. (1989) Ocean colour. Availability of the global data set. *EOS*, **70**, 634–641.

Fleming,R.H. (1957) General features of the ocean. *Geol. Soc. Am. Mem.*, **67**, 87–107.

Gessner,F. (1957) *Hydrobotanik. II. Stoffhaushalt.* Deutscher Verlag. Wiss., Berlin, p. 638.

Gieskes,W.W.C. and Kraay,G.W. (1986) Floristic and physiological differences between the shallow and the deep nanoplankton community in the euphotic zone of the open tropical Atlantic revealed by HPLC analysis of pigments. *Mar. Biol.*, **91**, 567–576.

Gieskes,W.W.C., Kraay,G.W., Nonji,A., Setiapermana,D. and Sutomo,L. (1988) Monsoonal alternations of a mixed and a layered structure in the phytoplankton of the Banda Sea (Indonesia): a mathematical analysis of algal pigment fingerprints. *Neth. J. Sea Res.*, **22**, 123–137.

Gloersen,P., Campbell,W.J., Cavalieri,D.J., Comiso,J.C., Parkinson,C.L. and Zwally,H.J. (1992) Arctic and Antarctic Sea Ice, 1978–1987. *NASA, Washington, Spec. Publ.*, **511**, 1–290.

Gordon,H.R. (1993) Radiative transfer in the atmosphere for correction of ocean color remote sensors. In Barale,V. and Schlittenhardt,P.M. (eds), *Ocean Colour: Theory and Applications in a Decade of CZCS Experience*. Kluwer Academic Publishers, Brussels, pp. 33–78.

Gordon,H.R. and Clark,D.K. (1980) Atmospheric effects in the remote sensing of phytoplankton pigments. *Boundary-Layer Meteorol.*, **18**, 299–313.

Gordon,H.R. and McCluney,W.R. (1975) Estimation of the depth of sunlight penetration in the sea for remote sensing. *Appl. Optics*, **14**, 413–416.

Gordon,H.R., Clark,D.K., Brown,J.W., Brown,O.B., Evans,R.H. and Broenkow,W.W. (1983) Phytoplankton pigment concentrations in the Middle Atlantic Bight: comparison of ship determinations and CZCS estimates. *Appl. Optics*, **22**, 20–36.

Hahn,C.J., Warren,S.G., London,J. and Chervin,R.M. (1987) Climatological data for clouds over the globe from surface observations. *Rep. Carbon Dioxide Inf. Cent. Oak Ridge*, NDP–026.

Head,E.J.H. and Horne,E.P.W. (1993) Pigment transformation and vertical flux in an area of convergence in the North Atlantic Ocean. *Deep-Sea Res.*, **40**, 329–346.

Houry,S., Dombrowsky,E., de Mey,P. and Minster,J.-F. (1987) Brunt-Väisälä frequency and Rossby radii in the South Atlantic. *J. Phys. Oceanogr.*, **17**, 1619–1626.

ICES (1958) Measurements of primary production in the sea. *Rapp P.-V. Réun.*, **144**, p. 158.
Knauer,G.A. (1993) Productivity and new production of the oceanic system. In Wollast,R. (ed.), *Interactions of C,N,P and S Biogeochemical Cycles and Global Change*. Springer-Verlag, Berlin, pp. 211–231.
Koblentz-Mishke,O.J. (1965) Magnitude of primary production of the Pacific Ocean. *Oceanology*, **5**, 325–337.
Koblentz-Mishke,O.J.L., Volkovinsky,V.V. and Kabanova,J.G. (1970) Plankton primary production of the world ocean. In Wooster,W.S. (ed.), *Scientific Exploration of the South Pacific*. National Academy of Sciences, Washington, DC, pp. 183–193.
Legendre,L., Ackley,S.F., Dieckmann,G.S., Gulliksen,B., Horner,R., Hoshiai,T., Melnikov,I.A., Reeburgh,W.S., Spindler,M. and Sullivan,C.W. (1992) Ecology of sea ice biota. 2. Global significance. *Polar Biol.*, **12**, 429–444.
Letelier,R.M., Bidigare,R.R., Hebel,D.V. and Ondrusek,M. (1993) Temporal variability of phytoplankton community structure based on pigment analysis. *Limn. Oceanogr.*, **38**, 1420–1437.
Lewis,M., Harrison,W.G., Oakey,N.S. Hebert,D. and Platt,T. (1986) Vertical nitrate fluxes in the oligotrophic ocean. *Science*, **234**, 870–873.
Longhurst,A.R. *Ecological Geography of the Ocean*. Academic Press, San Diego, CA, in preparation.
Love,C.M. (ed.) (1971) *EASTROPAC Atlas. US Dep. Comm. Circ.* 330.
Lukas,R. and Lindstrom,J. (1991) The mixed layer of the western equatorial Pacific Ocean. *J. Geophys. Res.*, **96**, 3343–3357.
Lurin,B., Rasool,S.I., Cramer,W. and Moore,B. (1994) Global terrestrial net primary production. *Glob. Change Newsl. (IGBP)*, **19**, 6–8.
Martin,J.H., Knauer,G.A., Karl,D.M. and Broenkow,W.W. (1987) VERTEX: carbon cycling in the northeast Pacific. *Deep-Sea Res.*, **34**, 323.
Mills,E. (1989) *Biological Oceanography. An Early History, 1870–1960*. Cornell University Press, Ithaca, 387 pp.
Mittelstaedt,E. (1991) The ocean boundary along the northwest African coast: circulation and oceanographic properties at the sea surface. *Prog. Oceanogr.*, **26**, 307–355.
Morel,A. (1980) In-water and remote measurement of ocean colour. *Boundary-Layer Meteorol.*, **18**, 177–201.
Morel,A. and Berthon,J.-F. (1989) Surface pigments, algal biomass profiles and potential production of the euphotic layer: Relationship reinvestigated in view of remote-sensing applications. *Limnol. Oceanogr.*, **34**, 1545–1562.
Morel,A. and Prieur,L. (1977) Analysis of variations in ocean colour. *Limnol. Oceanogr.*, **22**, 709–722.
Mueller,J.L. and Lang,R.E. (1989) Bio-optical provinces of the Northeast Pacific Ocean; A provisional analysis. *Limnol. Oceanogr.*, **34**, 1572–1586.
Osborne,J., Swift,J. and Flinchem,E.P (1992) *Ocean Atlas for the Macintosh*. Scripps Inst. Oceanogr. Ref. 92–29.
Parsons,T.R. and Lalli,C.M. (1988) Comparative oceanic ecology of the plankton community of the subarctic Atlantic and Pacific Oceans. *Oceanogr. Mar. Biol. Annu. Rev.*, **26**, 317–359.
Platt,T. (1984) Primary productivity in the central North Pacific: comparison to oxygen and carbon fluxes. *Deep-Sea Res.*, **31**, 1311–1319.
Platt,T. (1986) Primary production in the ocean water column as a function of surface light intensity *Deep-Sea Res.*, **33**, 149–163.
Platt,T. and Herman,A.W. (1983) Remote sensing of phytoplankton in the sea: surface layer chlorophyll as an estimate of water column chlorophyll and primary production. *Int. J. Remote Sens.*, **4**, 343–351.
Platt,T. and Sathyendranath,S. (1988) Oceanic primary production: estimation by remote sensing at local and regional scales. *Science*, **241**, 1613–1620.
Platt,T. and Subba Rao,D.V. (1975) Primary production of marine microphytes. In *Photosynthesis and Productivity in Different Environments*. Cambridge University Press, Cambridge, pp. 249–280.
Platt,T., Gallegos,C.L. and Harrison,W.G. (1980) Photoinhibition of photosynthesis in natural assemblages of marine phytoplankton. *J. Mar. Res.*, **38**, 687–701.
Platt,T., Sathyendranath,S., Caverhill,C.M. and Lewis,M.R. (1988) Ocean primary production and available light: further algorithms for remote sensing. *Deep-Sea Res.*, **35**, 855–879.
Platt,T., Harrison,W.G., Lewis,M.R., Li,W.K.W., Sathyendranath,S., Smith,R.E. and Vézina,A.F. (1989) Biological production of the oceans: the case for a consensus. *Mar. Ecol. Prog. Ser.*, **52**, 77–88.
Platt,T., Caverhill,C. and Sathyendranath,S. (1991) Basin-scale estimates of oceanic primary production by remote sensing: the North Atlantic. *J. Geophys. Res.*, **96**, 15147–15159.
Platt,T., Sathyendranath,S. and Longhurst,A.R. (1995) Remote sensing of primary production in the ocean: promise and fulfillment. *Phil. Trans. R. Soc. London Ser. A*, in press.

Riley,G.A. (1939) Plankton Studies. II. The western North Atlantic, May–June, 1939. *J. Mar. Res.*, **2**, 145–162.

Ryther,J.H. (1969) Photosynthesis and fish production in the sea. *Science*, **166**, 72–76.

Sathyendranath,S. and Morel,A. (1983) Light emerging from the sea—interpretations and uses in remote sensing. In Cracknell,A.P. (ed.), *Remote Sensing Applications in Marine Science and Technology*. D.Reidel, Dordrecht, pp. 323–357.

Sathyendranath,S. and Platt,T. (1989) Remote sensing of ocean chlorophyll: consequences of non-uniform pigment profile. *Appl. Optics*, **28**, 490–495.

Sathyendranath,S., Platt,T., Horne,E.P.W., Harrison,W.G., Ulloa,O., Outerbridge,R. and Hoepffner,N. (1991) Estimation of new production in the ocean by compound remote sensing. *Nature*, **353**, 129–133.

Sathyendranath,S., Longhurst,A.R., Caverhill,C.M. and Platt,T. (1995) Regionally and seasonally differentiated primary production in the North Atlantic. *Deep-Sea Res.*, in press.

Simpson,J.J. (1993) The Coastal Zone Colour Scanner (CZCS) algorithm. A critical review of residual problems. In Barale,V. and Schlittenhardt,P.M. (eds), *Ocean Colour: Theory and Applications in a Decade of CZCS Experience*. Kluwer Academic Publishers, Brussels, pp. 117–166.

Smith,R.C. (1981) Remote sensing and depth distribution of ocean chlorophyll. *Mar. Ecol. Prog. Ser.*, **5**, 359–361.

Steeman Nielsen,E. (1952) The use of radioactive carbon (C14) for measuring organic production in the sea. *J. Cons. Int. Explor. Mer*, **18**, 117–140.

Steeman Nielsen,E. and Jensen,E.A. (1957) The autotrophic production of organic matter in the oceans. *Galathea Rep.*, **1**, 49–124.

Strom,S.L. and Welschmeyer,N.A. (1991) Pigment-specific rates of phytoplankton growth and microzooplankton grazing in the open subarctic Pacific Ocean. *Limnol. Oceanogr.*, **36**, 50–63.

Sundquist,E.T. (1985) Geological perspectives on carbon dioxide and the carbon cycle. *Geophys. Monogr.*, **32**, 5–59.

Sverdrup,H.U. (1953) On the conditions for vernal blooming of the phytoplankton. *J. Cons. Perm. Int. Explor. Mer*, **18**, 287–295

Venrick,E.L. (1979) The lateral extent and characteristics of the North Pacific Central environment at 35N. *Deep-Sea Res.*, **26**, 1153–1178.

Woodwell,G.M., Rich,P.H. and Hall,C.A. (1973) Carbon in estuaries. *U.S. Atom. Energ. Comm. Symp. Ser.*, **30**, 221–239.

Received on November 15, 1994; accepted on February 6, 1995